Surface Functionalization of Nanoparticles with Polyethylene Glycol: Effects on Protein Adsorption and Cellular Uptake

Beatriz Pelaz,[†,¶] Pablo del Pino,[‡,¶] Pauline Maffre,[§,¶] Raimo Hartmann,[†] Marta Gallego,[‡] Sara Rivera-Fernández,[∥] Jesus M. de la Fuente,[⊥] G. Ulrich Nienhaus,[*,§,#] and Wolfgang J. Parak[*,†,‡]

[†]Fachbereich Physik, Philipps Universität Marburg, 35037 Marburg, Germany, [‡]CIC biomaGUNE, 20009 San Sebastian, Spain, [§]Institute of Applied Physics and Institute of Toxicology and Genetics, Karlsruhe Institute of Technology (KIT), Karlsruhe, Germany, [∥]Instituto de Nanociencia de Aragon, University of Zaragoza, 50018 Zaragoza, Spain, [⊥]Instituto de Ciencia de Materiales de Aragon, CSIC/University of Zaragoza, 50018 Zaragoza, Spain, and [#]Department of Physics, University of Illinois at Urbana—Champaign, Urbana, Illinois 61801, United States. [¶]B.P., P.d.P, and P.M. contributed equally to this work.

ABSTRACT Here we have investigated the effect of enshrouding polymer-coated nanoparticles (NPs) with polyethylene glycol (PEG) on the adsorption of proteins and uptake by cultured cells. PEG was covalently linked to the polymer surface to the maximal grafting density achievable under our experimental conditions. Changes in the effective hydrodynamic radius of the NPs upon adsorption of human serum albumin (HSA) and fibrinogen (FIB) were measured *in situ* using fluorescence correlation spectroscopy. For NPs without a PEG shell, a thickness increase of around 3 nm, corresponding to HSA monolayer adsorption, was measured at high HSA concentration. Only 50% of this value was found for NPs with PEGylated surfaces. While the size increase clearly reveals formation of a protein corona also for PEGylated NPs, fluorescence lifetime measurements and quenching experiments suggest that the adsorbed HSA molecules are buried within the PEG shell. For FIB adsorption onto PEGylated NPs, even less change in NP diameter was observed. *In vitro* uptake of the NPs by 3T3 fibroblasts was reduced to around 10% upon PEGylation with PEG chains of 10 kDa. Thus, even though the PEG coatings did not completely prevent protein adsorption, the PEGylated NPs still displayed a pronounced reduction of cellular uptake with respect to bare NPs, which is to be expected if the adsorbed proteins are not exposed on the NP surface.

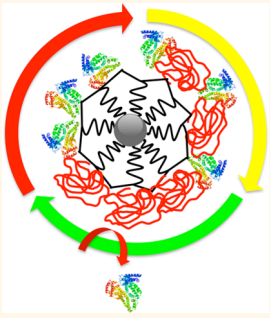

KEYWORDS: nanoparticle · polyethylene glycol · protein corona · fluorescence correlation spectroscopy · human serum albumin · fibrinogen · polymer coating

Colloidal nanoparticles (NPs) come into contact with the biological environment *via* their surfaces.[1−4] Thus, for biomedical applications, NP surfaces need to be carefully designed to elicit the desired effect, such as targeting to specific epitopes. By contrast, other applications may demand that NPs are not recognized by the environment, for example, to avoid their clearance by the immune system. To endow NPs with such "stealth" properties, modification of their surfaces with polyethylene glycol (PEG) has become a popular method. It reduces NP uptake by cultured cells *in vitro*[5−11] and by entire organisms *in vivo*, so that retention times of NPs in the blood circulation are increased.[12−17] These effects are often "explained" by postulating that PEGylation prevents formation of a protein corona and, thus, NPs are not recognized by the immune system. Indeed, there is experimental evidence supporting a reduced tendency of proteins to adsorb onto PEGylated surfaces, for example, by using mass spectrometry or gel electrophoresis.[9,18−20] In general, dense PEG coatings, which can vary with respect to the molecular weight and grafting density of the polymer, reduce the adsorption of opsonins *in vivo*.[21,22] The formation of an opsonin corona would immediately alert the phagocyte system,[23] thereby promoting rapid clearance of the NP−opsonin complex from the bloodstream. Likewise, PEGylation of NPs has been used traditionally *in vitro* to reduce nonspecific interactions with serum proteins,[11,24−26] which typically results in a reduced uptake by cultured cells compared with uptake of their non-PEGylated counterparts.[27] That said,

* Address correspondence to uli@uiuc.edu, wolfgang.parak@physik.uni-marburg.de.

Received for review March 1, 2015 and accepted June 16, 2015.

Published online June 16, 2015
10.1021/acsnano.5b01326

the formation of a protein corona can also hinder the interaction of NP ligands with the cellular membrane, resulting in a reduced uptake.[28]

The problem of protein adsorption onto PEGylated surfaces has attracted enormous attention of many researchers in the context of planar surfaces.[29−35] It has become clear that protein adsorption strongly depends on the density of PEGylation as well as on the molecular weight of the PEG chains employed.[9,30,32,36] The highest grafting density of PEG on surfaces can be obtained by growing PEG chains from monomers *in situ*, thereby ensuring a tight surface coverage.[18,37,38] Such layers are very efficient in preventing protein adsorption, especially when using long PEG chains. If PEG polymers are covalently attached to a surface,[18,39,40] the grafting density is limited by the PEG chain entropy, which drives PEG into a random coil shape, thereby hindering a close spacing of anchoring groups on the surface.[37,41] Proteins may penetrate less dense PEG layers, reside in voids,[42] and even approach and interact with the underlying reactive surfaces. Accordingly, an efficient strategy to prevent protein penetration into PEG layers has been to use star-shaped PEGs with reactive ends that allow dense cross-linking of the PEG surface layer.[43−45] Densely grafted, planar PEGylated surfaces have been reported to completely suppress protein adsorption but only in certain configurations.[41,46,47]

These findings are also of great relevance for studies of protein adsorption onto the spherical surfaces of PEGylated NPs. Most often, NPs are PEGylated by covalently binding entire PEG chains to NP surfaces, which limits the grafting density to values below those achieved by *in situ* growth. For such cases, it was shown that surface-bound PEG chains are coiled rather than stretched, resulting in a packing density below the theoretical maximum.[48,49] In addition, the curvature of the NP surface also has an effect on the density of surface ligands, as has been discussed in detail for the linkage of oligonucleotides to NP surfaces.[50,51] Thus, protein adsorption resistance of NPs can vary greatly, depending on the PEGylation strategy employed. However, even with reduced polymer surface density and, thus, presumably less than optimal protein-repellent coating, PEGylated NPs have shown markedly increased *in vivo* blood circulation retention times[14] as well as reduced *in vitro* NP uptake by cells.[52,53]

The protein-repellent nature of the NP surface is not the only effect of PEGylation. Other important physicochemical parameters of the NPs are likewise affected.[54] Most obvious is a change in size, as measured by the hydrodynamic radius.[49] Indeed, a NP size increase above a certain threshold, ~50 nm in the case of citric-acid-stabilized Au NPs, has been reported to reduce NP incorporation by cultured cells.[55] PEGylation can also modify the surface charge of NPs, even if nominally uncharged PEG molecules (*e.g.*, with a terminal hydroxy or methoxy group) are used. This effect may result from a reduction of the number of charged groups on the NP surface if they are, in part, utilized as anchoring points for PEG linkage and also due to chelation of cations by the PEG chains.[48] Such a reduction in surface charge may affect colloidal stability. Often, NPs are stabilized in solution by electrostatic repulsion, and they may lose colloidal stability due to charge screening by counterions at physiological salt concentrations (ionic strength around 150 mM).[56] PEGylation, however, confers colloidal stability to NPs *via* steric repulsion, even under high salt conditions.[57] Increase in colloidal stability has been linked to a decrease in NP uptake by cells *in vitro*.[52] To summarize, besides changes in surface chemistry, PEGylation of a NP has three distinct additional effects: (1) it increases its size and (2) its colloidal stability, and (3) it may reduce its surface charge density. All three effects typically lead to less efficient incorporation by cells.[58] Therefore, to better understand the effect of PEGylation on nano−bio interactions of NPs, it is important to disentangle the effect of reduced protein adsorption from direct effects on the physicochemical properties of the NPs.

In this study, we have quantitatively investigated protein adsorption on well-characterized PEGylated and non-PEGylated NPs. These NPs have an inorganic core and are coated with a shell of an amphiphilic polymer with integrated fluorophores, making them colloidally highly stable and, at the same time, endowing them with bright fluorescence emission.[59] The polymer-coated NPs can be conveniently PEGylated by linking PEG chains to the NPs' surface, resulting in a coiled PEG geometry.[48,49] They show reduced uptake by cells *in vitro*[52] as well as enhanced blood circulation retention times *in vivo*.[14] We have previously quantified protein adsorption onto similar NPs (without PEG) *in situ*,[60−62] employing fluorescence correlation spectroscopy (FCS).[63] In these model studies, we had dissolved the NPs in buffer solutions, in which individual protein species such as serum albumin or transferrin were present in well-defined concentrations varying over several orders of magnitude. Toward higher protein concentrations, monolayers of proteins were observed to adsorb onto the NPs in the cases of human serum albumin,[60,62,64] transferrin,[61] apolipoprotein A-I,[62] apolipoprotein E3,[65] apolipoprotein E4,[62] and complement component 3.[65] The strength of the NP−protein interaction could be characterized by the midpoint of the binding transition, that is, an apparent dissociation coefficient, K_d'. In the present work, these techniques are applied to PEGylated NPs. Hereby we have used two proteins for our investigation: human serum albumin (HSA) and fibrinogen (FIB). Both are abundant in blood and are interesting model systems due to their different size (HSA: triangular prism of sides 8.4 nm and thickness 3.15 nm;[66] FIB: 5 nm × 5 nm × 45 nm)

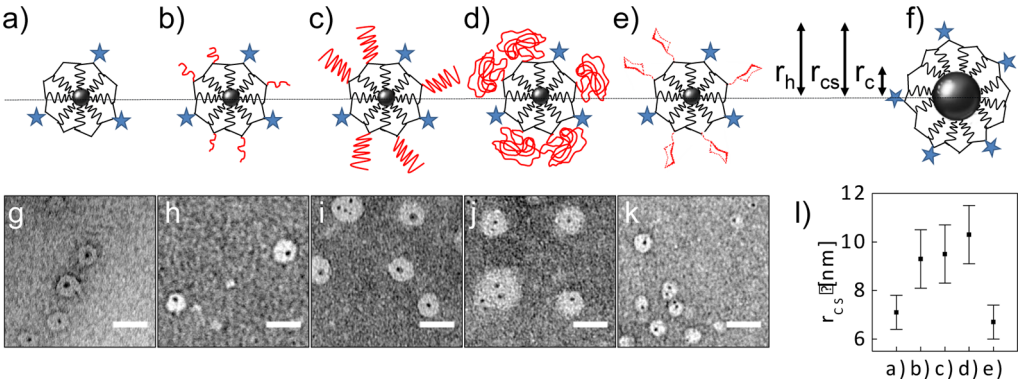

Figure 1. Sketch of the different NP samples studied in this work. All NPs contain an inorganic core with radius r_c, represented by a black sphere in the center. They are coated with the amphiphilic polymer poly(maleic anhydride-*alt*-dodecene) (PMA), to which the fluorophore DY-636 (drawn in light blue) was linked covalently.[59] PEG chains of different M_w or glucose (drawn in red) were linked to the NP surfaces, resulting in different hydrodynamic radii r_h: (a) FePt-PMA, (b) FePt-PMA-PEG750, (c) FePt-PMA-PEG5k, (d) FePt-PMA-PEG10k, (e) FePt-PMA-glucose, (f) Fe_3O_4-PMA. The bottom panels show selected regions of interest of negatively stained TEM micrographs (scale bar: 25 nm) for (g) FePt-PMA, (h) FePt-PMA-PEG750, (i) FePt-PMA-PEG5k, (j) FePt-PMA-PEG10k, and (k) FePt-PMA-glucose. (l) Comparison of the mean core−shell radius r_{cs} of the FePt samples, as determined by negative staining TEM analysis (data were derived from the images shown in Supporting Information, Figures I.10−I.14).

TABLE 1. Physicochemical Parameters of the Different NPs[a]

sample	(a)	(b)	(c)	(d)	(e)	(f)
NP core	FePt	FePt	FePt	FePt	FePt	Fe_3O_4
shell composition on top of PMA layer		PEG (750 Da)	PEG (5 kDa)	PEG (10 kDa)	glucose	
r_c [nm] (TEM)	1.6 ± 0.2	1.6 ± 0.2	1.6 ± 0.2	1.6 ± 0.2	1.6 ± 0.2	4.0 ± 0.6
r_{cs} [nm] (TEM)	7.1 ± 0.7	9.3 ± 1.2	9.5 ± 1.2	10.3 ± 1.2	6.7 ± 0.7	
r_h [nm] (DLS)	4.2 ± 0.2	4.8 ± 0.5	6.5 ± 0.7	10.6 ± 0.9	4.6 ± 0.6	6.2 ± 0.2
r_h [nm] (FCS)	5.4 ± 0.1	6.5 ± 0.1	7.9 ± 0.2	9.7 ± 0.2	5.4 ± 0.1	6.7 ± 0.2
ζ [mV]	−44 ± 3	−17.8 ± 0.5	−28 ± 1	−14.3 ± 0.4	−25 ± 3	−55 ± 3

[a] NPs consisting of an inorganic core, PMA polymer, and PEG/glucose shell, with inorganic core radii r_c (TEM) and geometric core/shell radii r_{cs} (TEM, negative staining), as determined in the dried state. The hydrodynamic radii r_h of the different NPs were measured in water by DLS (number distribution) and in phosphate-buffered saline without divalent ions (PBS, pH = 7.4) by FCS (shown is the fit parameter $r_h(0)^{(fit)}$). Zeta-potentials, ζ, were determined in water using LDA (number distribution). All raw data are included in the Supporting Information.

and due to their different apparent dissociation coefficient, K_d', which has been investigated in the literature in the context of the Vroman effect.[67−70]

RESULTS AND DISCUSSION

Schematic depictions of all NP samples used in this study are shown in Figure 1. The most important experimentally determined physicochemical parameters of the NPs are compiled in Table 1.

As expected, PEGylation leads to an increase in NP size (TEM (negative staining), dynamic light scattering (DLS), and FCS) and, concomitantly, to a reduction in the magnitude of surface charge laser Doppler anemometry (LDA); that is, they are less negatively charged. Considering that a single PEG monomeric unit is 44 Da in weight and 0.35 nm in length, the contour lengths of our PEG chains (*i.e.*, the length of PEG in hypothetically fully stretched conformation), with M_w of 750 Da, 5 kDa, and 10 kDa, amount to, respectively, 6, 40, and 80 nm. However, the hydrodynamic radius increase upon PEGylation is only between 1 and 6 nm for the three different PEG chains. These results clearly indicate that the PEG chains are not stretched, but coil, fold, or twist on the NP surface, in full agreement with previous reports.[49] In fact, the size increase with PEG weight rather scales with the radius of gyration of free PEG in its random coil conformation (see Supporting Information for details).[49] For FePt-PMA-glucose, no size increase was observed, but there was a reduction in surface charge, as for the PEGylated NPs. In contrast, NPs with bigger cores (Fe_3O_4 instead of FePt, *i.e.*, Fe_3O_4-PMA) had an increased hydrodynamic radius but maintained a surface charge similar to those with smaller cores but without PEGylation. Thus, the two control samples, one with an increased hydrodynamic radius but similar surface charge (Fe_3O_4−PMA) and the other one with a reduced surface charge but similar hydrodynamic radius (FePt-PMA-glucose), enabled us to separate effects specific for PEG surface functionalization from changes in basic physicochemical properties accompanying PEGylation, namely, changes in size and surface charge.

Colloidal stability of all NPs was probed by additional DLS studies. No significant size increase was found in NaCl solutions of different concentrations, demonstrating the high colloidal stability of all the NPs. Therefore, our NPs were well-dispersed and did not show

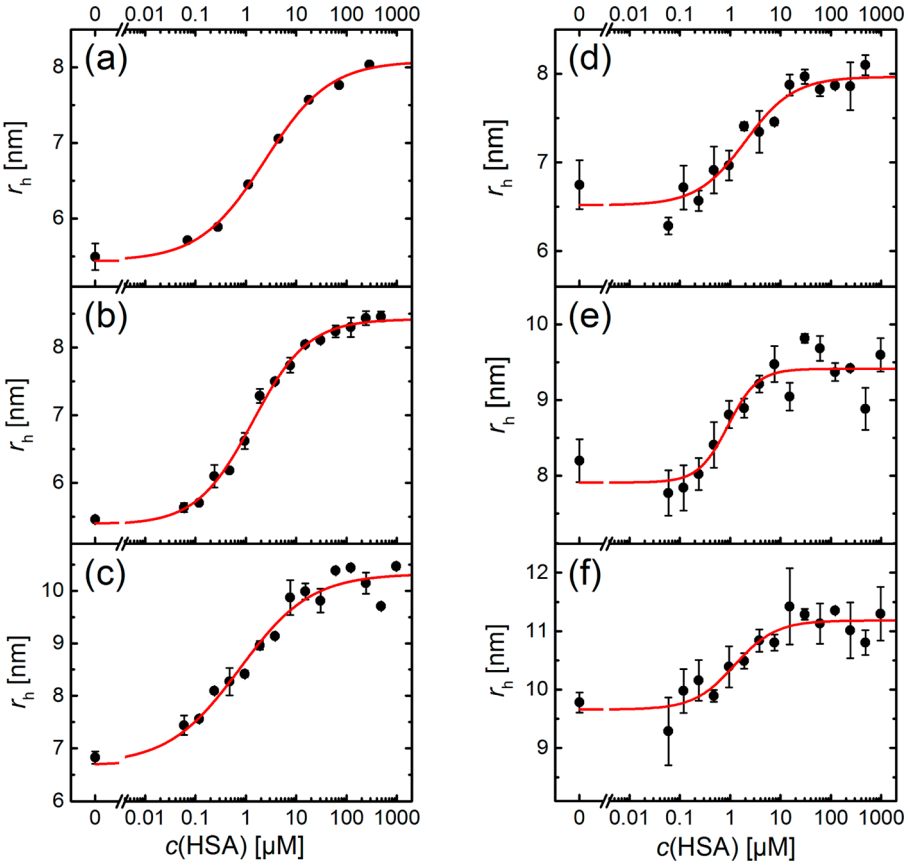

Figure 2. Hydrodynamic radius r_h of the different NP species, determined as a function of HSA concentration in PBS, and the corresponding fits based on the Hill model: (a) FePt-PMA, (b) FePt-PMA-glucose, (c) Fe_3O_4-PMA, (d) FePt-PMA-PEG750, (e) FePt-PMA-PEG5k, (f) FePt-PMA-PEG10k. The fit parameters are shown in Table 2.

noticeable agglomeration tendency, in good agreement with previous data concerning the colloidal stability of PMA-coated NPs (see the Supporting Information for data).[71,72]

Due to the integrated fluorophores, FCS can be conveniently used to measure diffusion coefficients of the NPs in the presence of proteins *in situ*, without any interference due to unbound proteins emitting background fluorescence.[60,73−75] The different NPs were incubated in PBS with varying concentrations of HSA. At each concentration, c, the resulting hydrodynamic radius of the NPs with adsorbed proteins, $r_h(c)$, was determined *via* FCS using a previously reported confocal microscope.[62] The resulting $r_h(c)$ curves were fitted using a model based on the volume of the adsorbed proteins, the number of which is described by the Hill equation (see Supporting Information)[60,73] (Figure 2), leading to the following fit parameters for each type of NP: hydrodynamic radius $r_h(0)$ of the NPs in the absence of proteins, increase in hydrodynamic radius Δr_h upon saturating the NP surface with HSA, Hill coefficient n, the maximum number N_{max} of HSA molecules bound per NP at saturation, and apparent dissociation coefficient K_d' (*i.e.*, the free protein concentration at which $N_{max}/2$ HSA molecules are bound to the NP on average). The results are summarized in Table 2.

The HSA adsorption onto the polymer-coated FePt NPs was found to be in good agreement with our previous reports; only the overall radius increase upon HSA binding to non-PEGylated FePt NPs was slightly smaller than in previous studies.[60,62] For all PEGylated NP preparations, the size likewise increased with increasing protein concentration, indicating that HSA associates with our PEGylated NPs. The binding affinity, which is inversely related to the apparent equilibrium dissociation coefficient K_d', was similar for PEGylated and non-PEGylated NPs (FePt-PMA-PEG *versus* FePt-PMA). The size increase due to HSA corona formation was only ~1.5 nm for the FePt-PMA-PEG NPs and thus reduced by roughly a factor of 2 from the values obtained for the non-PEGylated NPs (FePt-PMA, FePt-PMA-glucose, Fe_3O_4-PMA). This is a very interesting result because the obtained thickness, 1.5 nm, is less than the smallest extension of HSA (~3 nm). This finding may be explained in two different ways: either fewer HSA proteins bind to PEGylated NPs than to non-PEGylated NPs, or a similar number of HSA proteins may be adsorbed, but they may partially penetrate into the PEG layers of PEGylated NPs, resulting in repulsion of hydration water and, consequently, a denser coating layer than for FePt-PMA NPs. Both possibilities will be discussed below. Notably, the PEG chain length in our

TABLE 2. Compilation of Parameters As Obtained from a Least-Squares Fit of the Protein Adsorption Model to the FCS Data in Figure 2[a]

NP core	FePt	FePt	FePt	FePt	FePt	Fe_3O_4
surface modification		PEG (750 Da)	PEG (5 kDa)	PEG (10 kDa)	glucose	
$r_h(0)$ [nm]	5.5 ± 0.2	6.7 ± 0.3	8.2 ± 0.3	9.8 ± 0.2	5.5 ± 0.1	6.8 ± 0.2
$r_h(0)^{(fit)}$ [nm]	5.4 ± 0.1	6.5 ± 0.1	7.9 ± 0.2	9.7 ± 0.2	5.4 ± 0.1	6.7 ± 0.4
Δr_h [nm]	2.6 ± 0.1	1.4 ± 0.2	1.5 ± 0.3	1.5 ± 0.3	3.0 ± 0.1	3.6 ± 0.5
$r_h(c_{max})^{(fit)}$ [nm]	8.1 ± 0.1	7.9 ± 0.1	9.4 ± 0.2	11.2 ± 0.2	8.4 ± 0.1	10.3 ± 0.3
K_d' [μM]	4.1 ± 0.8	2.0 ± 1.0	1.0 ± 0.4	1.4 ± 0.7	2.3 ± 0.3	1.5 ± 0.5
N_{max}	15.2 ± 0.8	9.0 ± 1.0	14.0 ± 2.0	21.0 ± 3.0	18.3 ± 0.7	33.0 ± 4.0
n	0.7 ± 0.1	0.9 ± 0.3	1.5 ± 0.8	1.1 ± 0.5	0.8 ± 0.1	0.6 ± 0.2
$N_{max}/4\pi r_h^2(0)^{(fit)}$ [nm^{-2}]	0.041 ± 0.003	0.017 ± 0.002	0.018 ± 0.003	0.018 ± 0.003	0.050 ± 0.003	0.06 ± 0.01
$4\pi r_h^2(0)^{(fit)}/N_{max}$ [nm^2]	24 ± 2	59 ± 7	56 ± 9	56 ± 9	20 ± 1	17 ± 3

[a] $r_h(0)$ is the hydrodynamic radius of the NPs directly in PBS without HSA added. $r_h(0)^{(fit)}$ is the size of the NPs without HSA added, as obtained from fitting the measured $r_h(c)$ data points with the model described in Supporting Information. The fit also returns the parameters K_d', N_{max}, Δr_h, and n, which are the apparent dissociation coefficient, maximum number of proteins bound per NP, corona thickness, *i.e.*, the difference in radius of NPs saturated with proteins and NPs without proteins, and the Hill coefficient, respectively. $r_h(c_{max})^{(fit)} = r_h(0)^{(fit)} + \Delta r_h$ is the hydrodynamic radius of the NPs saturated with HSA. $N_{max}/4\pi r_h^2(0)^{(fit)}$ is the number of HSA proteins adsorbed onto a NP per unit of surface area, which is assumed to be $4\pi r_h^2(0)^{(fit)}$. The mean surface area occupied per bound protein is given in the last row (*i.e.*, the inverse of $N_{max}/4\pi r_h^2(0)^{(fit)}$).

case had no influence on the HSA binding affinity (K_d') nor on the HSA corona thickness (Δr_h), which is somehow at variance with other studies.[76]

As pointed out in the introduction, modified protein adsorption upon PEGylation could simply arise from the size increase of the PEGylated NPs. For this reason, we studied bigger, PMA-coated NPs without PEGylation as a control. Because a well-controlled procedure to increase the core size of our FePt NPs was not available, we instead employed Fe_3O_4 NPs with a bigger core diameter, but with exactly the same PMA polymer coating. Considering that the inorganic cores (FePt, Fe_3O_4) are completely buried in the polymer shell, we can reasonably presume that both types of NPs are essentially identical with respect to their surface properties. This view is also supported by the ζ-potentials of both NPs (FePt-PMA, Fe_3O_4-PMA), which are identical within the experimental error (Table 1). The data in Table 2 show that the size increase of the smaller FePt-PMA NPs and the bigger Fe_3O_4-PMA NPs upon saturation with HSA (Δr_h) is very similar, corresponding to a monolayer of HSA proteins. However, since the surface area of the Fe_3O_4-PMA NPs is greater than that of the FePt-PMA NPs, the number of adsorbed HSA molecules per NP (N_{max}) is increased. Therefore, we have calculated the number of proteins per surface area ($N_{max}/4\pi r_h^2(0)^{(fit)}$) (Table 2). This number is identical for FePt-PMA and Fe_3O_4-PMA NPs. Thus, the size increase of PMA-coated NPs from $r_h(0)^{(fit)}$ = 5.4 nm to $r_h(0)^{(fit)}$ = 6.7 nm did not affect HSA protein adsorption. In contrast, when the surface chemistry was modified by PEGylation, a significant change in the interactions can be seen. The Fe_3O_4-PMA and FePt-PMA-PEG750 samples have essentially identical hydrodynamic radii $r_h(0)^{(fit)}$ and, thus, identical surface areas. This result clearly shows that the reduced thickness change due to HSA adsorption, Δr_h, upon PEGylation is directly correlated with the specific properties of the PEG shell and not related to the accompanying change in NP size (within the size range investigated here).

The FePt-PMA-glucose NPs[20] showed HSA adsorption properties comparable to those of the FePt-PMA NPs, although their ζ-potential was reduced and more similar to the ζ-potentials measured for PEGylated NPs. Currently, neither the precise number of glucose molecules attached per NP nor their location and orientation on the surface is known. Certainly, the geometry of the glucose molecules on the NP surface is expected to play an important role. In fact, if they are partly buried in the polymer shell, a protein-repellent effect may be absent. Despite this lack of knowledge about their surface structure, the FePt-PMA-glucose NPs serve here as an important control. Like the PEGylated NPs, they had a reduced surface charge. However, glucose modification did not change the hydrodynamic radius, and the same amount of HSA adsorbed onto FePt-PMA-glucose NPs as onto FePt-PMA NPs (in terms of N_{max} as well as $N_{max}/4\pi r_h^2(0)^{(fit)}$). Thus, the change in protein adsorption that we have observed for the PEGylated samples does not result from a reduction in surface charge accompanying PEGylation but has to be ascribed definitively to the intrinsic properties of the PEG layer.

The two control experiments demonstrate that there is a specific effect of PEG to reduce Δr_h upon adsorption of HSA. To explain this reduction, we may consider two scenarios. First, we can hypothesize that the PEG layer remains unchanged upon protein adsorption, so proteins cannot penetrate. Based on this assumption, more protein molecules (as given by N_{max}) would adsorb onto the non-PEGylated than on the PEGylated NPs. This is also reflected in the normalized numbers, $N_{max}/4\pi r_h^2(0)^{(fit)}$, in which the surface density of HSA under saturation conditions is less than half that for PEGylated *versus* non-PEGylated NPs. One thus could state that the degree of adsorption of HSA molecules onto PEGylated NPs is only 50% (with the number of

adsorbed HSA molecules normalized to the surface area, $N_{max}/4\pi r_h^2(0)^{(fit)}$) of the value observed for non-PEGylated NPs. Upon PEGylation, the thickness of the protein corona (Δr_h) also would be only around 50% of the one around non-PEGylated NPs. However, data obtained with PEGylated flat surfaces suggest that a second scenario may also be plausible. Proteins are known to be attracted to PEG layers by short-range forces.[77] If they are sufficiently small, they may penetrate the PEG layer and get trapped inside the polymer layer.[78] Larger proteins, by contrast, may interact with the outer part of the PEG layer and compress it.[79] Under this assumption, there could be a similar amount of proteins adsorbed to the non-PEGylated *versus* the PEGylated NPs. In the case of PEGylated NPs, however, there would be a reduced increase in Δr_h, as HSA has partly penetrated the PEG layer and, possibly, even compressed the PEG layer.

Structural information, that is, knowledge about the geometry of the PEG layer after HSA adsorption, is required to resolve these issues experimentally. In the case of flat surfaces, the thickness of PEG layers has been determined with X-ray photoelectron spectroscopy (XPS), ellipsometry,[37] and atomic force microscopy (AFM).[80] Direct structural information about the location of proteins has been obtained with reflectometric interference spectroscopy (RIfS) and neutron reflectometry.[81] The reflectometry studies revealed that proteins can only penetrate into PEG layers of low grafting density. In this work, however, we are dealing with strongly curved NP surfaces, to which the above-mentioned techniques are difficult to apply. We were thus not able to quantitatively determine the geometry of the PEG layer on the NP surface. The key parameter of interest would be the grafting density of PEG, that is, the number of PEG molecules per NP surface area. Depending on the grafting density, PEG layers are known to have different geometry, changing from a mushroom-like structure to a brush-like structure at higher grafting density.[82,83] Differences in the conformation of the PEG layers have been demonstrated to directly affect protein adsorption[84,85] and NP uptake by cells.[86,87] In the case of the NPs used here, taking into account the reaction conditions (*i.e.*, the concentration of PEG during the attachment to the NP surface), we estimate that the PEG molecules are nondensely adsorbed in a mushroom conformation (see Supporting Information for detailed calculations). Our FCS data permit a precise determination of Δr_h but do not yield any other structural information. The gel electrophoresis data (shown in Supporting Information) indicate that, under our experimental conditions, no more PEG can be added to the NPs; that is, the NP surface is saturated with PEG. However, these data do not provide detailed structural information. Furthermore, the dense appearance of the PEG layers in TEM images using negative staining (Figure 1) is not suitable to obtain quantitative structural information.

To further address two key structural questions, whether protein adsorption changes the PEG conformation on our NPs and where the proteins are located upon adsorption, we employed fluorescence lifetime measurements and quenching experiments. Optical properties of fluorophores are sensitive to their physicochemical environment. Solvatochromism is one such example, where a shift in the absorption and emission peaks occurs in response to a change in fluorophore environment.[88] Medium conditions, however, may also affect the fluorescence lifetime.[89,90] We observed that adsorption of HSA onto the polymer shell of NPs increases the fluorescence lifetime of the integrated fluorophore DY-636 (see Supporting Information for data). If the PEG shell around the polymer-coated NPs is so dense that HSA molecules cannot penetrate the PEG layer, they would not reach the underlying polymer coating. Thus, the adsorption of HSA should not affect the lifetime of DY-636 in the polymer shell. However, we have observed a significant fluorescence lifetime increase of the DY-636 dye molecules in the polymer shell upon HSA binding that was similar for PEGylated and non-PEGylated NPs. This result supports our view that HSA molecules enter the PEG layer and bind to the negatively charged polymer surface (for a full discussion of these data, refer to the Supporting Information). Additional experiments using potassium iodide as a fluorescence quencher lend further support to this claim (Supporting Information). Thus, although we cannot provide direct structural evidence, our fluorescence spectroscopy data strongly suggest that HSA at least partly penetrates the PEG layer, which explains the reduced increase of Δr_h upon NP incubation with HSA. In this scenario, HSA molecules reside within the PEG coating of the NP rather than on the NP surface.

In order to probe whether the observed results are specific for HSA or also hold true for other serum proteins, we also studied the adsorption of FIB by FCS. FIB is a much larger protein than HSA, with a molecular weight of 340 kDa. It plays a major role in the formation of blood clots, which are formed through the polymerization of thrombin-truncated fibrinogen molecules called fibrins. The molecular structure of fibrinogen consists of pairs of α-, β-, and γ-chains, each containing 562, 461, and 411 amino acid residues. In its elongated, sigmoidal structure, FIB has overall molecular dimensions of $5 \times 5 \times 45$ nm^3 (as obtained from its crystallographic structure, PDB accession code 3GHG, with PyMol), corresponding to a volume of 1125 nm^3.[91] In previous studies, it has already been demonstrated that PEGylation reduces FIB adsorption.[79] The increase in hydrodynamic diameter of FePt-PMA and FePt-PMA-PEG10k NPs upon FIB adsorption, as measured here by using FCS, is shown in Figure 3 and Table 3. First, the

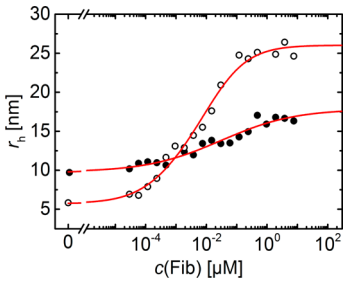

Figure 3. Hydrodynamic radius r_h of FePt-PMA (open circles) and FePt-PMA-PEG10k NPs (filled circles), measured as a function of FIB concentration in PBS, and the corresponding fits based on the Hill model. The fit parameters are shown in Table 3.

TABLE 3. Compilation of Parameters Obtained from a Least-Squares Fit of the Protein Adsorption Model to the FCS Data on FIB Displayed in Figure 3[a]

NP core	FePt	FePt
surface modification		PEG (10 kDa)
$r_h(0)^{(fit)}$ [nm]	5.8 ± 0.6	9.8 ± 0.5
Δr_h [nm]	20.0 ± 1.0	8.1 ± 1.6
$r_h(c_{max})^{(fit)}$ [nm]	26.0 ± 0.7	18.0 ± 1.0
K_d' [μM]	0.03 ± 0.01	0.14 ± 0.04
N_{max}	65 ± 5	18 ± 4
n	0.7 ± 0.1	0.4 ± 0.1
$N_{max}/4\pi r_h^2(0)^{(fit)}$ [nm^{-2}]	0.15 ± 0.03	0.015 ± 0.004
$4\pi r_h^2(0)^{(fit)}/N_{max}$ [nm^2]	6.4 ± 1.4	67.0 ± 16

[a] The parameters are the same as those in Table 2.

data obtained with non-PEGylated NPs confirm the much higher binding affinity of FIB on the same surface than HSA (K_d'(FIB) = 0.03 μM *versus* K_d'(HSA) = 4.1 μM for FePt-PMA NPs). This is the reason why HSA adsorbed to surfaces in contact with blood can be displaced by FIB. Second, the hydrodynamic radius increase $r_h(c_{max})^{(fit)}$ upon FIB adsorption is markedly smaller for the FePt-PMA-PEG10k NPs than for the non-PEGylated NPs, which clearly indicates reduced protein adsorption.

The crystal structure of FIB reveals a rod-like protein with a length of ~45 nm. The FCS data of FIB adsorbing onto FePt-PMA NPs in Figure 3 show only a radius increase of 20 nm, which may—at first sight—seem at odds with binding of such a large rod-like protein. FIB is overall negatively charged but has two pronounced patches of positive charge at either end of the rod, through which it may adsorb onto the negatively charged NPs.[92] FIB is known to be quite flexible, and we assume that the rod can bend, so that both positively charge ends come into contact with the NP surface. In this conformation, a bound FIB molecule would have a bow-like structure, which would rise to the observed radius increase $\Delta r_h \approx 20$ nm (see Supporting Information for a structural depiction). The maximum number of FIB molecules bound, N_{max} = 65 ± 5, which is obtained from the binding model assuming that the entire volume of the adsorption layer is taken up by FIB proteins, appears somewhat large. More realistically, one may estimate this parameter by dividing the overall NP surface by the size of the "footprint" of a single FIB molecule (~5 × 3 nm^2), which results in a smaller number, N_{max} = 28 ± 6, of FIB molecules binding per NP.

FIB also associates with PEGylated NP surfaces, as clearly inferred from the size increase observed with FePt-PMA-PEG10k NPs (Figure 3), which is also in agreement with findings by others.[93] However, the affinity of FIB binding to PEGylated NPs is markedly lower in comparison to that of FePt-PMA NPs (K_d' = 0.14 μM for FePt-PMA-PEG10k *versus* K_d' = 0.03 μM for FePt-PMA), and the thickness of the FIB corona is significantly reduced (Δr_h = 8.1 nm for FePt-PMA-PEG10k *versus* Δr_h = 20.0 nm for FePt-PMA). It seems very unlikely that the reduction in Δr_h upon FIB adsorption onto PEGylated NPs is a result of a smaller number of adsorbed FIB molecules on the outer surface of the PEG shell. FIB molecules most likely penetrate the nondense PEG layer and bind to the polymer PMA surfaces. FIB adsorption causes a compression of the PEG molecules, so that further FIB proteins cannot adsorb to such areas of locally increased PEG density. Consequently, an effective number of FIB binding sites on the FePt-PMA-PEG10k NPs is reduced, as suggested by the measured protein corona thickness of only about 8 nm. Based on the fits to the binding data (Figure 3), N_{max} calculated from the volume of the protein shell is reduced by about 70% (N_{max} = 65 *vs* N_{max} = 18). Estimating the number of FIB molecules *via* the available surface area, a 70% decrease would correspond to only 8 ± 2 binding sites (rather than 28 ± 6 for the non-PEGylated FePt-PMA NPs). The FIB data also indicate that adsorbed proteins are able to penetrate the PEG shell of PEGylated NPs.

In order to assess the biological activity of PEG present on the surface of our NPs, we investigated the effect of the different coatings (PEG, glucose) on the internalization of NPs by cultured cells from the NIH/3T3 murine fibroblast cell line (ATCC, #CRL-1658). 3T3 cells were incubated for 12 h (37 °C, 5% CO_2) with Dulbecco's modified Eagle's medium (DMEM) supplemented with 10% fetal bovine serum and containing NPs at 5 or 10 nM concentrations (for details, see Supporting Information). Note that serum-containing culture conditions will cause the formation of a protein corona around the NPs, which reduces NP uptake by cells as compared to serum-free culture conditions.[61] Then, the cells were fixed and stained in blue with 4′,6-diamidino-2-phenylindole (DAPI) and the cell membrane in green with wheat germ agglutinin (WGA)-Alexa 488. Images of the cells were recorded by using confocal microscopy. Besides the blue (DAPI) and green (WGA-Alexa 488) fluorescence channels, we also recorded red fluorescence originating from the DY-636-labeled polymer coating around the NPs.

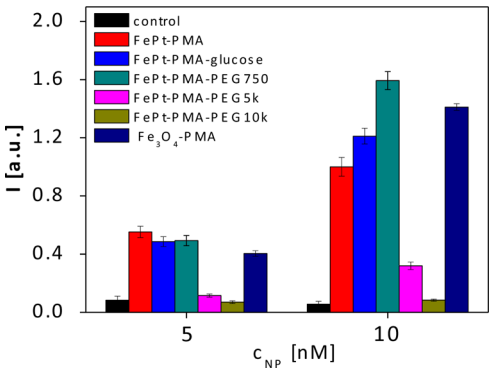

Figure 4. Integrated NP fluorescence *I* per cell (mean value ± standard deviation, obtained from 150−500 cells) after having incubated 3T3 fibroblasts in serum-containing medium with NPs at concentrations c_{NP} = 5 or 10 nM. The intensity of Fe_3O_4 NPs was scaled with the ratio *R* (0.67) of the fluorescence per FePt NP to the fluorescence per Fe_3O_4 NP. The control sample refers to the residual fluorescence of 3T3 cells without added NPs.

With custom-made software written in Matlab (Mathworks), individual cells were automatically identified and masked, based on the nuclei/membrane staining as described in Supporting Information. Algorithms for cell detection and segmentation were provided by the open source software CellProfiler.[94] Then, the mean fluorescence intensity originating from NP emission within each cell mask (*i.e.*, the mean signal of all pixels corresponding to NPs inside one single cell) was determined and multiplied by the area of the cell. In this way, the integrated fluorescence *I* of each cell (=mean pixel intensity within the cell × cross section area of the cell) was determined (Figure 4). The obtained value can be taken as proportional to the total uptake of NPs per cell because the height of the imaged plane relative to the growth surface was kept constant (Supporting Information). The results are presented as average integrated fluorescence per cell. NPs adhering to the outer plasma membrane may contribute to the overall signal; however, we removed these NPs as thoroughly as possible by extensive washing before imaging. The fluorescence of non-internalized particles attached to the outer plasma membrane is negligible, as judged from inspection of the collected images (Supporting Information).

Because the fluorescent dyes were incorporated in the PMA polymer shell around the FePt core prior to further modification by PEG and glucose, these samples can be compared based on the fluorescence intensity in the cell samples. Also, FCS measurements verified that NP brightness did not change upon PEGylation. For the Fe_3O_4 NPs, however, the core and thus the amount of PMA shell is larger and so is the number of fluorophores per NP. To normalize the fluorescence such that the signal reflects the number of NPs regardless of the size, the fluorescence intensity, *I*, of the Fe_3O_4 NPs was scaled with the ratio *R* of the fluorescence per FePt NP to the fluorescence per Fe_3O_4 NP ($R = I_{FePt}/I_{Fe_3O_4}$). This scaling factor was determined either by measuring the fluorescence intensity of solutions of PMA-coated FePt and Fe_3O_4 NPs with equal concentrations (R = 0.67, see the Supporting Information) or by assuming that the number of fluorophores scales with the surface area of the PMA-coating, as reported in Table 2: $R = r_h^2(0)^{(fit)}(\text{FePt-PMA})/r_h^2(0)^{(fit)}(Fe_3O_4\text{-PMA}) = (5.4\text{ nm})^2/(6.7\text{ nm})^2 \approx 0.64$. The intensity data of incorporated Fe_3O_4 NPs were then multiplied by the scaling factor R = 0.67 for comparison with the intensity data of FePt NPs, as shown in Figure 4. NP uptake depends on the NP size; typically, bigger NPs are incorporated to a lesser extent. For citric-acid-stabilized NPs, for example, it has been shown that the number of NPs incorporated by the cells is reduced with increasing size (for diameters >50 nm).[55] However, in our case, the difference in $r_h(0)$ between the NP samples is too small in relation to the experimental uncertainty to afford a definitive statement about the size dependence of cellular uptake. For glucose-modified NPs, we did not observe a reduction of uptake, although previous work (using a different cell line) has shown that functionalization of NPs with glucose can modify their uptake efficiency.[95] More specifically, glucose-functionalized NPs have been reported to be internalized into cells by lipid raft pathways instead of conventional clathrin-mediated endocytosis.[96]

Cellular uptake in serum-containing media is greatly reduced for our PEGylated FePt-PMA-PEG5k and -PEG10k NPs, whereas this trend is not observed or even inverted for FePt-PMA-PEG750 (*i.e.*, at 10 nM, the NP uptake was increased compared to the non-PEGylated NPs). Clearly, the effect is more pronounced for NPs covered with PEG of high M_w, in agreement with the literature.[6,9,97] While we cannot explain the increase in uptake of FePt-PMA-PEG750 as compared to FePt-PMA at 10 nM NP concentration, uptake of NPs covered with 10 kDa PEG (FePt-PMA-10 kDa PEG) is largely reduced to an amount as low as *ca.* 10% of the value for non-PEGylated NPs (FePt-PMA) (Figure 4). Uptake suppression is not due to the increased size upon PEGylation because the larger Fe_3O_4 control sample was incorporated to a greater degree. Thus, uptake reduction of PEGylated NPs is specific for the high molecular weight PEG coating.

The FCS data shown in Figures 2 and 3 demonstrate that PEGylation reduces the amount of HSA and FIB adsorbed to the FePt-PMA-based NPs. However, HSA and FIB adsorption was clearly not completely suppressed. Our data rather indicate that adsorbed proteins penetrate and deform the PEG layer, which was below the theoretical maximum coverage density. Although the PEG layer was not fully packed, cellular uptake of PEGylated NPs still was greatly reduced in serum-containing media. Fetal bovine serum (FBS), which was a component of the media used for the

cellular uptake studies, comprises thousands of different types of proteins. Thus, the question arises how representative our *in vitro* model studies of adsorption of a single serum protein (Figures 3 and 4) are for protein adsorption from serum-containing medium used in the cellular uptake studies. Here we present two arguments supporting a close inter-relation: First, in earlier work,[71] we performed NP uptake studies of similar NPs in FBS-supplemented media and in media enriched with HSA. In both cases, we observed the same tendency, that is, reduced NP uptake upon formation of a protein corona. Second, while not being able to emulate the full dynamic complexity[98] of a protein corona in serum-containing media or even in human blood plasma, HSA and FIB are key players in protein adsorption from blood onto surfaces.[68,99] The fast-adsorbing HSA is dynamically replaced by FIB, which especially makes FIB a key protein adsorbed onto the NP surface in equilibrium. Our data provide strong evidence that PEGylated NPs in serum-containing media, as typically used in NP uptake studies, are not devoid of a protein corona but that part of the adsorbed proteins penetrate and deform the PEG layer on the NP surface.

CONCLUSIONS

We have presented a systematic investigation of protein adsorption onto PEGylated, polymer-coated NPs. In this study, we have also included control NPs without PEG coating but with modified size and surface charge to prove that the observed effects result from the unique interaction properties of PEGylated surfaces rather than mere changes of NP size and surface charge. Even though the PEGs were grafted onto the NPs at high density (though still below the theoretically possible maximum coverage), this was clearly not sufficient to completely abolish protein adsorption. In fact, the small size of the NPs, giving rise to a strong surface curvature for obvious geometric reasons, requires an even denser surface grafting than for planar surfaces so as to efficiently prevent protein penetration into the PEG layer.

HSA was observed to bind to our various NPs with apparent affinities in the micromolar range, whereas FIB binding was observed to be 1−2 orders of magnitude stronger. Of note, the micromolar affinities of HSA adsorption reported here indicate that proteins form a rather weakly bound or soft corona around the NPs. Consequently, it is not possible to directly quantify the amount of adsorbed HSA *in situ* by commonly used techniques such as mass spectroscopy or gel electrophoresis because the required purification from unbound protein would disturb the dynamic equilibrium between free and NP-bound HSA proteins. Unlike most other approaches, the FCS method used here permits *in situ* measurements in thermal equilibrium.

Upon HSA binding, non-PEGylated NPs (FePt-PMA, FePt-PMA-glucose, Fe_3O_4-PMA) displayed a radius increase of ∼3 nm at saturation, which is consistent with formation of a monolayer of HSA on top of the NP surfaces, with the HSA molecules adsorbing with one of their triangular faces.[60] Of note, this size increase has been observed for chemically different, small NPs, as well.[64] In contrast, the size increase resulting from HSA adsorption was significantly reduced to ∼1.5 nm for our PEGylated NPs. This difference could, in principle, result from smaller numbers of binding sites for HSA molecules on top of the PEG layers enshrouding the NPs. However, we have gathered spectroscopic evidence, by using fluorescence lifetime analysis and quenching studies (with KI) of the DY-636 fluorophores attached to the NPs, strongly suggesting that HSA penetrates the PEG layer of our NPs and resides within the PEG layer. Presumably, they are adsorbed to the underlying surface to which the PEG chains are grafted. This result is in line with previous studies carried out on planar PEG layers, examining protein adsorption as a function of the grafting density and chain length of the PEG molecules forming the layer.[18,35,37] The results from our FIB binding data completely support this interpretation. The reduction of the thickness of the protein corona due to NP surface PEGylation is even smaller for FIB than for HSA adsorption. The large size of FIB makes it very unlikely that there is merely a reduced number of FIB molecules adsorbed per NP on the outer PEGylated surface. The data rather suggest that adsorbed FIB molecules penetrate and deform the PEG layer.

In agreement with previous studies, we have observed that PEGylation reduces NP uptake by cultured cells.[5,6,8,9,11,14,15,17] Whereas proteins were adsorbed onto the outer surface of the non-PEGylated NPs, proteins likely reside inside the PEG layer for PEGylated NPs. Therefore, the protein corona can be largely hidden from the interface, and the NPs continue to interact with cells *via* their PEG surfaces, even though proteins are adsorbed. Thus, for PEG coatings that are not grafted at the maximal coverage density, a dramatically reduced NP uptake by cells can be observed, and even protein adsorption is not completely suppressed through these coatings.

In regard to the future development of NP surface coatings, we stress that PEGylation may not always be the optimal strategy when developing devices for targeted drug delivery. Notably, for drug targeting *via* intravenous delivery, the two key consequences of PEGylation, namely, reduced cellular uptake and increased retention times, are conflicting. Long retention times in the body are highly desirable to obtain longer circulation of the NPs in the blood vessels, thus offering a higher chance to reach a tumor site, for example, by passive targeting *via* the enhanced permeation and retention effect. However, poor NP uptake by cells inside

tumor tissue due to PEGylation is not desirable.[100,101] Zwitterionic surfaces are presently discussed as promising alternatives,[65,102−107] ensuring extended retention times as well as enhanced NP internalization by cells. Thus, detailed studies of interactions of such NPs with proteins will be highly desirable for the future.

EXPERIMENTAL PROCEDURES

FePt NPs, with a radius of $r_c = 1.6 \pm 0.2$ nm in the inorganic core, were coated with an amphiphilic polymer based on poly(maleic anhydride-*alt*-dodecene) (PMA) labeled with the fluorescent dye DY-636 according to published protocols[60] (for details, refer to the Supporting Information). This polymer renders the NPs water-soluble by exposing carboxyl groups on the NP surface. The solution containing the polymer-coated NPs was purified from residual polymeric micelles by gel electrophoresis.[108] PEG chains of different molecular weight (M_w = 750 Da, 5 kDa, 10 kDa) were linked to the NP surfaces *via* standard bioconjugate chemistry (*i.e.*, *via* amide bond formation between terminal amino groups on the PEG chains and the carboxyl groups of the polymer) to the maximum extent possible, as confirmed by gel electrophoresis.[48] Negative TEM staining was used to determine the core−shell radius r_{cs} of the PEGylated NPs. We also prepared PMA-coated Fe_3O_4 NPs with a larger inorganic core radius, $r_c = 4.0 \pm 0.6$ nm (as determined by TEM), but without PEGylation as a control sample of NPs with different size. Furthermore, we prepared PMA-coated FePt NPs surface-modified with glucose as a control sample of NPs with a reduced surface charge.

All NPs were thoroughly characterized using transmission electron microscopy (TEM), inductively coupled plasma mass spectrometry (ICP-MS), UV/vis absorption and fluorescence spectroscopy, gel electrophoresis, dynamic light scattering (DLS), fluorescence correlation spectroscopy (FCS), and laser Doppler anemometry (LDA). The adsorption of HSA and FIB on the surface of the different NPs was quantitatively analyzed *in situ* by using FCS, yielding a precise determination of the hydrodynamic radius of the NPs with adsorbed proteins as a function of the protein concentration. A simple binding model allows us to compute the apparent equilibrium dissociation coefficient K_d', the maximum number of proteins N_{max} bound per NP, the corona thickness Δr_h, and the Hill coefficient n.[60] A similar approach has been attempted recently by others using DLS.[109] In addition, incorporation of the NPs by 3T3 cells was quantified *in vitro* by immunostaining and confocal microcopy.[110]

Conflict of Interest: The authors declare no competing financial interest.

Acknowledgment. B.P. acknowledges the Alexander von Humboldt Foundation for a postdoctoral fellowship. This work was supported by the Deutsche Forschungsgemeinschaft (GRK 1782 to W.J.P., GRK 2039 to G.U.N.), the European Research Council (Starting Grant 239931-NANOPUZZLE to J.M.dlF.), the European Commission (project Futurenanoneeds to W.J.P.), the MINECO (MAT2013-48169-R, NanoFATE, to W.J.P. and P.d.P.), and the KIT in the context of the Helmholtz STN Program (to G.U.N.). The authors are grateful to Karsten Kantner for determining NP concentrations by ICP-MS, and to Marco Möller for assistance in negative staining TEM.

Supporting Information Available: Synthesis of NPs, colloidal characterization of NPs, quantification of the adsorption of proteins, location of adsorbed human serum albumin and uptake of NPs by 3T3 fibroblasts. The Supporting Information is available free of charge on the ACS Publications website at DOI: 10.1021/acsnano.5b01326.

REFERENCES AND NOTES

1. Nel, A. E.; Madler, L.; Velegol, D.; Xia, T.; Hoek, E. M. V.; Somasundaran, P.; Klaessig, F.; Castranova, V.; Thompson, M. Understanding Biophysicochemical Interactions at the Nano-Bio Interface. *Nat. Mater.* **2009**, *8*, 543–557.
2. Monopoli, M. P.; Walczyk, D.; Campbell, A.; Elia, G.; Lynch, I.; Bombelli, F. B.; Dawson, K. A. Physical-Chemical Aspects of Protein Corona: Relevance to *in Vitro* and *in Vivo* Biological Impacts of Nanoparticles. *J. Am. Chem. Soc.* **2011**, *133*, 2525–2534.
3. Akesson, A.; Cardenas, M.; Elia, G.; Monopoli, M. P.; Dawson, K. A. The Protein Corona of Dendrimers: PAMAM Binds and Activates Complement Proteins in Human Plasma in a Generation Dependent Manner. *RSC Adv.* **2012**, *2*, 11245–11248.
4. Hamad, I.; Al-Hanbali, O.; Hunter, A. C.; Rutt, K. J.; Andresen, T. L.; Moghimi, S. M. Distinct Polymer Architecture Mediates Switching of Complement Activation Pathways at the Nanosphere−Serum Interface: Implications for Stealth Nanoparticle Engineering. *ACS Nano* **2010**, *4*, 6629–6638.
5. Zhang, Y.; Kohler, N.; Zhang, M. Q. Surface Modification of Superparamagnetic Magnetite Nanoparticles and Their Intracellular Uptake. *Biomaterials* **2002**, *23*, 1553–1561.
6. Xie, J.; Xu, C.; Kohler, N.; Hou, Y.; Sun, S. Controlled PEGylation of Monodisperse Fe_3O_4 Nanoparticles for Reduced Non-specific Uptake by Macrophage Cells. *Adv. Mater.* **2007**, *19*, 3163–3166.
7. Ryman-Rasmussen, J. P.; Riviere, J. E.; Monteiro-Riviere, N. A. Variables Influencing Interactions of Untargeted Quantum Dot Nanoparticles with Skin Cells and Identification of Biochemical Modulators. *Nano Lett.* **2007**, *7*, 1344–1348.
8. Hak, S.; Helgesen, E.; Hektoen, H. H.; Huuse, E. M.; Jarzyna, P. A.; Mulder, W. J. M.; Haraldseth, O.; Davies, C. L. The Effect of Nanoparticle Polyethylene Glycol Surface Density on Ligand-Directed Tumor Targeting Studied *in Vivo* by Dual Modality Imaging. *ACS Nano* **2012**, *6*, 5648–5658.
9. Gref, R.; Lück, M.; Quellec, P.; Marchand, M.; Dellacherie, E.; Harnisch, S.; Blunk, T.; Müller, R. H. 'Stealth' Corona-Core Nanoparticles Surface Modified by Polyethylene Glycol (PEG): Influences of the Corona (PEG Chain Length and Surface Density) and of the Core Composition on Phagocytic Uptake and Plasma Protein Adsorption. *Colloids Surf., B* **2000**, *18*, 301–313.
10. He, Q.; Zhang, J.; Shi, J.; Zhu, Z.; Zhang, L.; Bu, W.; Guo, L.; Chen, Y. The Effect of PEGylation of Mesoporous Silica Nanoparticles on Nonspecific Binding of Serum Proteins and Cellular Responses. *Biomaterials* **2010**, *31*, 1085–1092.
11. Dai, Q.; Walkey, C.; Chan, W. C. W. Polyethylene Glycol Backfilling Mitigates the Negative Impact of the Protein Corona on Nanoparticle Cell Targeting. *Angew. Chem., Int. Ed.* **2014**, *53*, 5093–5096.
12. Ballou, B.; Lagerholm, B. C.; Ernst, L. A.; Bruchez, M. P.; Waggoner, A. S. Noninvasive Imaging of Quantum Dots in Mice. *Bioconjugate Chem.* **2004**, *15*, 79–86.
13. Daou, T. J.; Li, L.; Reiss, P.; Josserand, V.; Texier, I. Effect of Poly(ethylene glycol) Length on the *in Vivo* Behavior of Coated Quantum Dots. *Langmuir* **2009**, *25*, 3040–3044.
14. Lipka, M.; Semmler-Behnke, M.; Sperling, R. A.; Wenk, A.; Takenaka, S.; Schleh, C.; Kissel, T.; Parak, W. J.; Kreyling, W. G. Biodistribution of PEG-Modified Gold Nanoparticles Following Intratracheal Instillation and Intravenous Injection. *Biomaterials* **2010**, *31*, 6574–6581.
15. von Maltzahn, G.; Park, J.-H.; Agrawal, A.; Bandaru, N. K.; Das, S. K.; Sailor, M. J.; Bhatia, S. N. Computationally Guided Photothermal Tumor Therapy Using Long-Circulating Gold Nanorod Antennas. *Cancer Res.* **2009**, *69*, 3892–3900.
16. Cho, W. S.; Cho, M.; Jeong, J.; Choi, M.; Han, B. S.; Shin, H. S.; Hong, J.; Chung, B. H.; Jeong, J.; Cho, M. H.

Size-Dependent Tissue Kinetics of PEG-Coated Gold Nanoparticles. *Toxicol. Appl. Pharmacol.* **2010**, *245*, 116–123.
17. Perrault, S. D.; Walkey, C.; Jennings, T.; Fischer, H. C.; Chan, W. C. W. Mediating Tumor Targeting Efficiency of Nanoparticles through Design. *Nano Lett.* **2009**, *9*, 1909–1915.
18. Kingshott, P.; Thissen, H.; Griesser, H. J. Effects of Cloud-Point Grafting, Chain Length, and Density of PEG Layers on Competitive Adsorption of Ocular Proteins. *Biomaterials* **2002**, *23*, 2043–2056.
19. Pasche, S.; De Paul, S. M.; Voros, J.; Spencer, N. D.; Textor, M. Poly(L-lysine)-graft-Poly(ethylene glycol) Assembled Monolayers on Niobium Oxide Surfaces: A Quantitative Study of the Influence of Polymer Interfacial Architecture on Resistance to Protein Adsorption by ToF-SIMS and *in Situ* OWLS. *Langmuir* **2003**, *19*, 9216–9225.
20. Moros, M.; Pelaz, B.; Lopez-Larrubia, P.; Garcia-Martin, M. L.; Grazu, V.; de la Fuente, J. M. Engineering Biofunctional Magnetic Nanoparticles for Biotechnological Applications. *Nanoscale* **2010**, *2*, 1746–1755.
21. Wattendorf, U.; Merkle, H. P. PEGylation as a Tool for the Biomedical Engineering of Surface Modified Microparticles. *J. Pharm. Sci.* **2008**, *97*, 4655–4669.
22. Pozzi, D.; Colapicchioni, V.; Caracciolo, G.; Piovesana, S.; Capriotti, A. L.; Palchetti, S.; De Grossi, S.; Riccioli, A.; Amenitsch, H.; Lagana, A. Effect of Polyethyleneglycol (PEG) Chain Length on the Bio-Nano-Interactions between PEGylated Lipid Nanoparticles and Biological Fluids: From Nanostructure to Uptake in Cancer Cells. *Nanoscale* **2014**, *6*, 2782–2792.
23. Gordon, D. L.; Rice, J. L. Opsonin-Dependent and Independent Surface Phagocytosis of *S. aureus* Proceeds Independently of Complement and Complement Receptors. *Immunology* **1988**, *64*, 709–714.
24. Waku, T.; Matsusaki, M.; Kaneko, T.; Akashi, M. PEG Brush Peptide Nanospheres with Stealth Properties and Chemical Functionality. *Macromolecules* **2007**, *40*, 6385–6392.
25. Orts-Gil, G.; Natte, K.; Thiermann, R.; Girod, M.; Rades, S.; Kalbe, H.; Thuenemann, A. F.; Maskos, M.; Oesterle, W. On the Role of Surface Composition and Curvature on Biointerface Formation and Colloidal Stability of Nanoparticles in a Protein-Rich Model System. *Colloids Surf., B* **2013**, *108*, 110–119.
26. Bargheer, D.; Nielsen, J.; Gebel, G.; Heine, M.; Salmen, S. C.; Stauber, R.; Weller, H.; Heeren, J.; Nielsen, P. The Fate of a Designed Protein Corona on Nanoparticles *in Vitro* and *in Vivo*. *Beilstein J. Nanotechnol.* **2015**, *6*, 36–46.
27. Torrisi, V.; Graillot, A.; Vitorazi, L.; Crouzet, Q.; Marletta, G.; Loubat, C.; Berret, J. F. Preventing Corona Effects: Multiphosphonic Acid Poly(ethylene glycol) Copolymers for Stable Stealth Iron Oxide Nanoparticles. *Biomacromolecules* **2014**, *15*, 3171–3179.
28. Treuel, L.; Brandholt, S.; Maffre, P.; Wiegele, S.; Shang, L.; Nienhaus, G. U. Impact of Protein Modification on the Protein Corona on Nanoparticles and Nanoparticle–Cell Interactions. *ACS Nano* **2014**, *8*, 503–513.
29. McPherson, T.; Kidane, A.; Szleifer, I.; Park, K. Prevention of Protein Adsorption by Tethered Poly(ethylene oxide) Layers: Experiments and Single-Chain Mean-Field Analysis. *Langmuir* **1998**, *14*, 176–186.
30. Michel, R.; Pasche, S.; Textor, M.; Castner, D. G. Influence of PEG Architecture on Protein Adsorption and Conformation. *Langmuir* **2005**, *21*, 12327–12332.
31. Pasche, S.; Vörös, J.; Griesser, H. J.; Spencer, N. D.; Textor, M. Effects of Ionic Strength and Surface Charge on Protein Adsorption at PEGylated Surfaces. *J. Phys. Chem. B* **2005**, *109*, 17545–17552.
32. Mrksich, M.; Whitesides, G. M. Using Self-Assembled Monolayers To Understand the Interactions of Man-Made Surfaces with Proteins and Cells. *Annu. Rev. Biophys. Biomol. Struct.* **1996**, *25*, 55–78.
33. Ostuni, E.; Chapman, R. G.; Holmlin, R. E.; Takayama, S.; Whitesides, G. M. A Survey of Structure–Property Relationships of Surfaces That Resist the Adsorption of Protein. *Langmuir* **2001**, *17*, 5605–5620.
34. Mrksich, M.; Chen, C. S.; Xia, Y.; Dike, L. E.; Ingber, D. E.; Whitesides, G. M. Controlling Cell Attachment on Contoured Surfaces with Self-Assembled Monolayers of Alkanethiolates on Gold. *Proc. Natl. Acad. Sci. U.S.A.* **1996**, *93*, 10775–10778.
35. Zhang, M.; Desai, T.; Ferrari, M. Proteins and Cells on PEG Immobilized Silicon Surfaces. *Biomaterials* **1998**, *19*, 953–960.
36. Jeon, S. I.; Lee, J. H.; Andrade, J. D.; De Gennes, P. G. Protein–Surface Interactions in the Presence of Polyethylene Oxide: I. Simplified Theory. *J. Colloid Interface Sci.* **1991**, *142*, 149–158.
37. Sofia, S. J.; Premnath, V.; Merrill, E. W. Poly(ethylene oxide) Grafted to Silicon Surfaces: Grafting Density and Protein Adsorption. *Macromolecules* **1998**, *31*, 5059–5070.
38. Piehler, J.; Brecht, A.; Valiokas, R.; Liedberg, B.; Gauglitz, G. A High-Density Poly(ethylene glycol) Polymer Brush for Immobilization on Glass-Type Surfaces. *Biosens. Bioelectron.* **2000**, *15*, 473–483.
39. Sheth, S. R.; Leckband, D. Measurements of Attractive Forces between Proteins and End-Grafted Poly(ethylene glycol) Chains. *Proc. Natl. Acad. Sci. U.S.A.* **1997**, *94*, 8399–8404.
40. Klapper, Y.; Vranceanu, M.; Ishitsuka, Y.; Evans, D.; Scheider, D.; Nienhaus, G. U.; Leneweit, G. Surface Energy of Phospholipid Bilayers and the Correlation to Their Hydration. *J. Colloid Interface Sci.* **2013**, *390*, 267–274.
41. Yang, Z.; Galloway, J. A.; Yu, H. Protein Interactions with Poly(ethylene glycol) Self-Assembled Monolayers on Glass Substrates: Diffusion and Adsorption. *Langmuir* **1999**, *15*, 8405–8411.
42. Heyes, C. D.; Kobitski, A. Y.; Amirgoulova, E. V.; Nienhaus, G. U. Biocompatible Surfaces for Specific Tethering of Individual Protein Molecules. *J. Phys. Chem. B* **2004**, *108*, 13387–13394.
43. Amirgoulova, E. V.; Groll, J.; Heyes, C. D.; Ameringer, T.; Röcker, C.; Möller, M.; Nienhaus, G. U. Biofunctionalized Polymer Surfaces Exhibiting Minimal Interaction towards Immobilized Proteins. *ChemPhysChem* **2004**, *5*, 552–555.
44. Groll, J.; Amirgoulova, E. V.; Ameringer, T.; Heyes, C. D.; Röcker, C.; Nienhaus, G. U.; Möller, M. , Biofunctionalized, Ultrathin Coatings of Cross-Linked Star-Shaped Poly(ethylene oxide) Allow Reversible Folding of Immobilized Proteins. *J. Am. Chem. Soc.* **2004**, *126*, 4234–4239.
45. Heyes, C. D.; Groll, J.; Möller, M.; Nienhaus, G. U. Synthesis, Patterning and Applications of Star-Shaped Poly(ethylene glycol) Biofunctionalized Surfaces. *Mol. BioSyst.* **2007**, *3*, 419–430.
46. Harder, P.; Grunze, M.; Dahint, R.; Whitesides, G. M.; Laibinis, P. E. Molecular Conformation in Oligo(ethylene glycol)-Terminated Self-Assembled Monolayers on Gold and Silver Surfaces Determines Their Ability To Resist Protein Adsorption. *J. Phys. Chem. B* **1998**, *102*, 426–436.
47. Wang, R. L. C.; Kreuzer, H. J.; Grunze, M. Molecular Conformation and Solvation of Oligo(ethylene glycol)-Terminated Self-Assembled Monolayers and Their Resistance to Protein Adsorption. *J. Phys. Chem. B* **1997**, *101*, 9767–9773.
48. Sperling, R. A.; Pellegrino, T.; Li, J. K.; Chang, W. H.; Parak, W. J. Electrophoretic Separation of Nanoparticles with a Discrete Number of Functional Groups. *Adv. Funct. Mater.* **2006**, *16*, 943–948.
49. Sperling, R. A.; Liedl, T.; Duhr, S.; Kudera, S.; Zanella, M.; Lin, C.-A. J.; Chang, W. H.; Braun, D.; Parak, W. J. Size Determination of (Bio-) Conjugated Water-Soluble Colloidal Nanoparticles: A Comparison of Different Techniques. *J. Phys. Chem. C* **2007**, *111*, 11552–11559.
50. Parak, W. J.; Pellegrino, T.; Micheel, C. M.; Gerion, D.; Williams, S. C.; Alivisatos, A. P. Conformation of Oligonucleotides Attached to Gold Nanocrystals Probed by Gel Electrophoresis. *Nano Lett.* **2003**, *3*, 33–36.
51. Pellegrino, T.; Sperling, R. A.; Alivisatos, A. P.; Parak, W. J. Gel Electrophoresis of Gold–DNA Nanoconjugates. *J. Biomed. Biotechnol.* **2007**, *2007*, 26796.

52. Brandenberger, C.; Mühlfeld, C.; Ali, Z.; Lenz, A.-G.; Schmid, O.; Parak, W. J.; Gehr, P.; Rothen-Rutishauser, B. Quantitative Evaluation of Cellular Uptake and Trafficking of Plain and Polyethylene Glycol-Coated Gold Nanoparticles. *Small* **2010**, *6*, 1669–1678.
53. Van Hoecke, K.; De Schamphelaer, K. A. C.; Ali, Z.; Zhang, F.; Elsaesser, A.; Rivera Gil, P.; Parak, W. J.; Smagghe, G.; Janssen, C. R. Ecotoxicity and Uptake of Polymer Coated Gold Nanoparticles. *Nanotoxicology* **2013**, *7*, 37–47.
54. Rivera Gil, P.; Jimenez de Aberasturi, D.; Wulf, V.; Pelaz, B.; del Pino, P.; Zhao, Y.; de la Fuente, J.; Ruiz de Larramendi, I.; Rojo, T.; Liang, X.-J.; et al. The Challenge To Relate the Physicochemical Properties of Colloidal Nanoparticles to Their Cytotoxicity. *Acc. Chem. Res.* **2013**, *46*, 743–749.
55. Chithrani, B. D.; Ghazan, A. A.; Chan, C. W. Determining the Size and the Shape Dependence of Gold Nanoparticle Uptake into Mammalian Cells. *Nano Lett.* **2006**, *6*, 662–668.
56. Pellegrino, T.; Kudera, S.; Liedl, T.; Javier, A. M.; Manna, L.; Parak, W. J. On the Development of Colloidal Nanoparticles towards Multifunctional Structures and Their Possible Use for Biological Applications. *Small* **2005**, *1*, 48–63.
57. Logie, J.; Owen, S. C.; McLaughlin, C. K.; Shoichet, M. S. PEG-Graft Density Controls Polymeric Nanoparticle Micelle Stability. *Chem. Mater.* **2014**, *26*, 2847–2855.
58. Nazarenus, M.; Zhang, Q.; Soliman, M. G.; del Pino, P.; Pelaz, B.; Carregal Romero, S.; Rejman, J.; Rothen-Ruthishauser, B.; Clift, M. J. D.; Zellner, R.; et al. *In Vitro* Interaction of Colloidal Nanoparticles with Mammalian Cells: What Have We Learned Thus Far? *Beilstein J. Nanotechnol.* **2014**, *5*, 1477–1490.
59. Zhang, F.; Lees, E.; Amin, F.; Rivera Gil, P.; Yang, F.; Mulvaney, P.; Parak, W. J. Polymer-Coated Nanoparticles: A Universal Tool for Biolabelling Experiments. *Small* **2011**, *7*, 3113–3127.
60. Röcker, C.; Pötzl, M.; Zhang, F.; Parak, W. J.; Nienhaus, G. U. A Quantitative Fluorescence Study of Protein Monolayer Formation on Colloidal Nanoparticles. *Nat. Nanotechnol.* **2009**, *4*, 577–580.
61. Jiang, X.; Weise, S.; Hafner, M.; Röcker, C.; Zhang, F.; Parak, W. J.; Nienhaus, G. U. Quantitative Analysis of the Protein Corona on FePt Nanoparticles Formed by Transferrin Binding. *J. R. Soc., Interface* **2010**, *7*, S5–S13.
62. Maffre, P.; Nienhaus, K.; Amin, F.; Parak, W. J.; Nienhaus, G. U. Characterization of Protein Adsorption onto FePt Nanoparticles Using Dual-Focus Fluorescence Correlation Spectroscopy. *Beilstein J. Nanotechnol.* **2011**, *2*, 374–383.
63. Nienhaus, G. U.; Maffre, P.; Nienhaus, K. Studying the Protein Corona on Nanoparticles by FCS. *Methods Enzymol.* **2013**, *519*, 115–137.
64. Maffre, P.; Brandholt, S.; Nienhaus, K.; Shang, L.; Parak, W. J.; Nienhaus, G. U. Effects of Surface Functionalization on the Adsorption of Human Serum Albumin onto Nanoparticles: A Fluorescence Correlation Spectroscopy Study. *Beilstein J. Nanotechnol.* **2014**, *5*, 2036–2047.
65. Klapper, Y.; Maffre, P.; Shang, L.; Ekdahl, K. N.; Nilsson, B.; Hettler, S.; Dries, M.; Gerthsen, D.; Nienhaus, G. U. Low Affinity Binding of Plasma Proteins to Lipid-Coated Quantum Dots As Observed by *in Situ* Fluorescence Correlation Spectroscopy. *Nanoscale* **2015**, *7*, 9980–9984.
66. Ferrer, M. L.; Duchowicz, R.; Carrasco, B.; de la Torre, J. G.; Acuña, A. U. The Conformation of Serum Albumin in Solution: A Combined Phosphorescence Depolarization-Hydrodynamic Modeling Study. *Biophys. J.* **2001**, *80*, 2422–2430.
67. Vroman, L. Effect of Adsorbed Proteins on Wettability of Hydrophilic and Hydrophobic Solids. *Nature* **1962**, *196*, 476–477.
68. Noh, H.; Vogler, E. A. Volumetric Interpretation of Protein Adsorption: Competition from Mixtures and the Vroman Effect. *Biomaterials* **2007**, *28*, 405–422.
69. Jung, S.-Y.; Lim, S.-M.; Albertorio, F.; Kim, G.; Gurau, M. C.; Yang, R. D.; Holden, M. A.; Cremer, P. S. The Vroman Effect: A Molecular Level Description of Fibrinogen Displacement. *J. Am. Chem. Soc.* **2003**, *125*, 12782–12786.
70. Hirsh, S. L.; McKenzie, D. R.; Nosworthy, N. J.; Denman, J. A.; Sezerman, O. U.; Bilek, M. M. M. The Vroman Effect: Competitive Protein Exchange with Dynamic Multilayer Protein Aggregates. *Colloids Surf., B* **2013**, *103*, 395–404.
71. Hühn, D.; Kantner, K.; Geidel, C.; Brandholt, S.; De Cock, I.; Soenen, S. J. H.; Rivera Gil, P.; Montenegro, J.-M.; Braeckmans, K.; Müllen, K.; et al. Polymer-Coated Nanoparticles Interacting with Proteins and Cells: Focusing on the Sign of the Net Charge. *ACS Nano* **2013**, *7*, 3253–3263.
72. Caballero-Díaz, E.; Pfeiffer, C.; Kastl, L.; Rivera Gil, P.; Simonet, B.; Valcárcel, M.; Jiménez-Lamana, J.; Laborda, F.; Parak, W. J. The Toxicity of Silver Nanoparticles Depends on Their Uptake by Cells and Thus on Their Surface Chemistry. *Part. Part. Syst. Charact.* **2013**, *30*, 1079–1085.
73. del Pino, P.; Pelaz, B.; Zhang, Q.; Maffre, P.; Nienhaus, G. U.; Parak, W. J. Protein Corona Formation around Nanoparticles: From the Past to the Future. *Mater. Horiz.* **2014**, *1*, 301–313.
74. Huang, R.; Carney, R. P.; Ikuma, K.; Stellacci, F.; Lau, B. L. T. Effects of Surface Compositional and Structural Heterogeneity on Nanoparticle–Protein Interactions: Different Protein Configurations. *ACS Nano* **2014**, *8*, 5402–5412.
75. Dominguez-Medina, S.; McDonough, S.; Swanglap, P.; Landes, C. F.; Link, S. *In Situ* Measurement of Bovine Serum Albumin Interaction with Gold Nanospheres. *Langmuir* **2012**, *28*, 9131–9139.
76. Dobrovolskaia, M. A.; Neun, B. W.; Man, S.; Ye, X.; Hansen, M.; Patri, A. K.; Crist, R. M.; McNeil, S. E. Protein Corona Composition Does Not Accurately Predict Hematocompatibility of Colloidal Gold Nanoparticles. *Nanomedicine* **2014**, *10*, 1453–1463.
77. Halperin, A. Polymer Brushes That Resist Adsorption of Model Proteins: Design Parameters. *Langmuir* **1999**, *15*, 2525–2533.
78. Gon, S.; Santore, M. M. Sensitivity of Protein Adsorption to Architectural Variations in a Protein-Resistant Polymer Brush Containing Engineered Nanoscale Adhesive Sites. *Langmuir* **2011**, *27*, 15083–15091.
79. Gon, S.; Bendersky, M.; Ross, J. L.; Santore, M. M. Manipulating Protein Adsorption Using a Patchy Protein-Resistant Brush. *Langmuir* **2010**, *26*, 12147–12154.
80. Park, H.-W.; Choi, J.; Ohn, K.; Lee, H.; Kim, J. W.; Won, Y.-Y. Study of the Air–Water Interfacial Properties of Biodegradable Polyesters and Their Block Copolymers with Poly(ethylene glycol). *Langmuir* **2012**, *28*, 11555–11566.
81. Schneck, E.; Schollier, A.; Halperin, A.; Moulin, M.; Haertlein, M.; Sferrazza, M.; Fragneto, G. Neutron Reflectometry Elucidates Density Profiles of Deuterated Proteins Adsorbed onto Surfaces Displaying Poly(ethylene glycol) Brushes: Evidence for Primary Adsorption. *Langmuir* **2013**, *29*, 14178–14187.
82. Backmann, N.; Kappeler, N.; Braun, T.; Huber, F.; Lang, H.-P.; Gerber, C.; Lim, R. Y. H. Sensing Surface PEGylation with Microcantilevers. *Beilstein J. Nanotechnol.* **2010**, *1*, 3–13.
83. Perry, J. L.; Reuter, K. G.; Kai, M. P.; Herlihy, K. P.; Jones, S. W.; Luft, J. C.; Napier, M.; Bear, J. E.; DeSimone, J. M. PEGylated PRINT Nanoparticles: The Impact of PEG Density on Protein Binding, Macrophage Association, Biodistribution, and Pharmacokinetics. *Nano Lett.* **2012**, *12*, 5304–5310.
84. Sacchetti, C.; Motamedchaboki, K.; Magrini, A.; Palmieri, G.; Mattei, M.; Bernardini, S.; Rosato, N.; Bottini, N.; Bottini, M. Surface Polyethylene Glycol Conformation Influences the Protein Corona of Polyethylene Glycol-Modified Single-Walled Carbon Nanotubes: Potential Implications on Biological Performance. *ACS Nano* **2013**, *7*, 1974–1989.
85. Lee, J. H.; Jeong, B. J.; Lee, H. B. Plasma Protein Adsorption and Platelet Adhesion onto Comb-like PEO Gradient Surfaces. *J. Biomed. Mater. Res.* **1997**, *34*, 105–114.

86. Rabanel, J.-M.; Hildgen, P.; Banquy, X. Assessment of PEG on Polymeric Particles Surface, a Key Step in Drug Carrier Translation. *J. Controlled Release* **2014**, *185*, 71–87.
87. Hafner, A. M.; Burschowsky, D.; Corthesy, B.; Textor, M.; Merkle, H. P. Surface Assembly of Poly(I:C) on PEGylated Microspheres to Shield from Adverse Interactions with Fibroblasts. *J. Controlled Release* **2012**, *159*, 204–214.
88. Amin, F.; Yushchenko, D. A.; Montenegro, J. M.; Parak, W. J. Integration of Organic Fluorophores in the Surface of Polymer-Coated Colloidal Nanoparticles for Sensing the Local Polarity of the Environment. *ChemPhysChem* **2012**, *13*, 1030–1035.
89. Choi, J. Y.; Park, E. J.; Chang, S. H.; Kang, T. J. Solvent Effects on the Solvatochromism of 7-Aminocoumarin Derivatives in Neat and Binary Solvent Mixtures: Correlation of the Electronic Transition Energies with the Solvent Polarity Parameters. *Bull. Korean Chem. Soc.* **2009**, *30*, 1452–1458.
90. Berezin, M. Y.; Lee, H.; Akers, W.; Achilefu, S. Near Infrared Dyes as Lifetime Solvatochromic Probes for Micropolarity Measurements of Biological Systems. *Biophys. J.* **2007**, *93*, 2892–2899.
91. Kollman, J. M.; Pandi, L.; Sawaya, M. R.; Riley, M.; Doolittle, R. F. Crystal Structure of Human Fibrinogen. *Biochemistry* **2009**, *48*, 3877–3886.
92. Deng, Z. J.; Liang, M.; Monteiro, M.; Toth, I.; Minchin, R. F. Nanoparticle-Induced Unfolding of Fibrinogen Promotes Mac-1 Receptor Activation and Inflammation. *Nat. Nanotechnol.* **2011**, *6*, 39–44.
93. Brambilla, D.; Verpillot, R.; Le Droumaguet, B.; Nicolas, J.; Taverna, M.; Kona, J.; Lettiero, B.; Hashemi, S. H.; De Kimpe, L.; Canovi, M.; et al. PEGylated Nanoparticles Bind to and Alter Amyloid-Beta Peptide Conformation: Toward Engineering of Functional Nanomedicines for Alzheimer's Disease. *ACS Nano* **2012**, *6*, 5897–5908.
94. Carpenter, A.; Jones, T.; Lamprecht, M.; Clarke, C.; Kang, I.; Friman, O.; Guertin, D.; Chang, J.; Lindquist, R.; Moffat, J.; et al. CellProfiler: Image Analysis Software for Identifying and Quantifying Cell Phenotypes. *Genome Biol.* **2006**, *7*, R100.
95. de la Fuente, J. M.; Alcantara, D.; Penades, S. Cell Response to Magnetic Glyconanoparticles: Does the Carbohydrate Matter? *IEEE Trans. Nanobiosci.* **2007**, *6*, 275–281.
96. Moros, M.; Hernáez, B.; Garet, E.; Dias, J. T.; Sáez, B.; Grazú, V.; González-Fernández, Á.; Alonso, C.; de la Fuente, J. M. Monosaccharides *versus* PEG-Functionalized NPs: Influence in the Cellular Uptake. *ACS Nano* **2012**, *6*, 1565–1577.
97. Harakeh, S.; Abdel-Massih, R. M.; Rivera Gil, P.; Sperling, R. A.; Meinhardt, A.; Niedwiecki, A.; Rath, M.; Parak, W. J.; Baydoun, E. The Effect of PEG-Coated Gold Nanoparticles on the Anti-proliferative Potential of Specific Nutrient Synergy. *Nanotoxicology* **2010**, *4*, 177–185.
98. Tenzer, S.; Docter, D.; Kuharev, J.; Musyanovych, A.; Fetz, V.; Hecht, R.; Schlenk, F.; Fischer, D.; Kiouptsi, K.; Reinhardt, C.; et al. Rapid Formation of Plasma Protein Corona Critically Affects Nanoparticle Pathophysiology. *Nat. Nanotechnol.* **2013**, *8*, 772–781.
99. Vroman, L.; Adams, A. L.; Fischer, G. C.; Munoz, P. C. Interaction of High Molecular Weight Kininogen, Factor XII, and Fibrinogen in Plasma at Interfaces. *Blood* **1980**, *55*, 156–159.
100. Zhang, G.; Yang, Z.; Lu, W.; Zhang, R.; Huang, Q.; Tian, M.; Li, L.; Liang, D.; Li, C. Influence of Anchoring Ligands and Particle Size on the Colloidal Stability and *in Vivo* Biodistribution of Polyethylene Glycol-Coated Gold Nanoparticles in Tumor-Xenografted Mice. *Biomaterials* **2009**, *30*, 1928–1936.
101. Duan, X.; Li, Y. Physicochemical Characteristics of Nanoparticles Affect Circulation, Biodistribution, Cellular Internalization, and Trafficking. *Small* **2013**, *9*, 1521–1532.
102. Zhou, W.; Shao, J.; Jin, Q.; Wei, Q.; Tang, J.; Ji, J. Zwitterionic Phosphorylcholine as a Better Ligand for Gold Nanorods Cell Uptake and Selective Photothermal Ablation of Cancer Cells. *Chem. Commun.* **2010**, *46*, 1479–1481.
103. Murthy, A. K.; Stover, R. J.; Hardin, W. G.; Schramm, R.; Nie, G. D.; Gourisankar, S.; Truskett, T. M.; Sokolov, K. V.; Johnston, K. P. Charged Gold Nanoparticles with Essentially Zero Serum Protein Adsorption in Undiluted Fetal Bovine Serum. *J. Am. Chem. Soc.* **2013**, *135*, 7799–7802.
104. Muro, E.; Pons, T.; Lequeux, N.; Fragola, A.; Sanson, N.; Lenkei, Z.; Dubertret, B. Small and Stable Sulfobetaine Zwitterionic Quantum Dots for Functional Live-Cell Imaging. *J. Am. Chem. Soc.* **2010**, *132*, 4556–4557.
105. Wang, T.; Bai, J.; Jiang, X.; Nienhaus, G. U. Cellular Uptake of Nanoparticles by Membrane Penetration: A Study Combining Confocal Microscopy with FTIR Spectroelectrochemistry. *ACS Nano* **2012**, *6*, 1251–1259.
106. Jiang, X.; Röcker, C.; Hafner, M.; Nienhaus, G. U. Endo- and Exocytosis of Zwitterionic Quantum Dot Nanoparticles by Living Cells. *ACS Nano* **2010**, *4*, 6787–6797.
107. Breus, V. V.; Heyes, C. D.; Tron, K.; Nienhaus, G. U. Zwitterionic Biocompatible Quantum Dots for Wide pH Stability and Weak Nonspecific Binding to Cells. *ACS Nano* **2009**, *3*, 2573–2580.
108. Fernández-Argüelles, M. T.; Yakovlev, A.; Sperling, R. A.; Luccardini, C.; Gaillard, S.; Medel, A. S.; Mallet, J.-M.; Brochon, J.-C.; Feltz, A.; Oheim, M.; et al. Synthesis and Characterization of Polymer-Coated Quantum Dots with Integrated Acceptor Dyes as FRET-Based Nanoprobes. *Nano Lett.* **2007**, *7*, 2613–2617.
109. Cui, M.; Liu, R.; Deng, Z.; Ge, G.; Liu, Y.; Xie, L. Quantitative Study of Protein Coronas on Gold Nanoparticles with Different Surface Modifications. *Nano Res.* **2014**, *7*, 345–352.
110. Schweiger, C.; Hartmann, R.; Zhang, F.; Parak, W. J.; Kissel, T.; Rivera Gil, P. Quantification of the Internalization Patterns of Superparamagnetic Iron Oxide Nanoparticles with Opposite Charge. *J. Nanobiotechnol.* **2012**, *10*, 28.